Article

Numerical Simulation and Structure Optimization of Multilayer Metamaterial Plus-Shaped Solar Absorber Design Based on Graphene and SiO$_2$ Substrate for Renewable Energy Generation

Haitham Alsaif [1] , **Shobhit K. Patel [2]** , **Naim Ben Ali [3,4,*]** , **Ammar Armghan [5,*]** and **Khaled Aliqab [5]**

1   Department of Electrical Engineering, College of Engineering, University of Ha'il,
    Ha'il City 81451, Saudi Arabia
2   Department of Computer Engineering, Marwadi University, Rajkot 360003, India
3   Department of Industrial Engineering, College of Engineering, University of Ha'il,
    Ha'il City 81451, Saudi Arabia
4   Photovoltaic and Semiconductor Materials Laboratory, National Engineering School of Tunis, University of Tunis El Manar, Tunis 1002, Tunisia
5   Department of Electrical Engineering, College of Engineering, Jouf University, Sakaka 72388, Saudi Arabia
*   Correspondence: na.benali@uoh.edu.sa (N.B.A.); aarmghan@ju.edu.sa (A.A.); Tel.: +966-595569515 (N.B.A.)

Abstract: Renewable energy is the energy for future generations as it is clean and widely available. The solar absorber is a sustainable energy source that converts solar energy into heat energy. The structural optimization is analyzed to enhance the absorption of the multilayer design. The proposed efficient solar absorber is made of a multilayer plus-shaped resonator supported by a SiO$_2$ substrate with a graphene spacer. The multilayer approach is utilized to enhance the absorption of the overall structure. The absorption of the multilayer solar absorber design is presented with AM 1.5 response observing the amount of energy absorbed from solar radiation. The different structural parameters are optimized to obtain the efficiency plus-shaped absorber design. The results of a different angle of incidence clearly show that the absorber is giving high absorption over a wide-angle range. The design results are also being analyzed with other similar works to show the improvement. The proposed absorber with high efficiency will be a good choice for solar thermal energy conversion applications.

Keywords: structural optimization; broadband; numerical; metasurface; graphene; absorption

MSC: 65-11; 68U07; 78-10; 78A40; 78M50; 90C31

1. Introduction

Renewable energy is getting the attention of researchers because it is a non-polluted and abundantly available resource compared to its counterpart fossil fuels. The solar absorber is a renewable source that converts solar radiation into heat and that heat can be used for several applications. Solar absorbers are used in solar water heaters, solar drying, etc. The efficiency of solar absorbers is a critical issue and researchers are working on increasing it. One of the ways to increase efficiency is by absorbing major solar radiation covering the range of infrared, visible, and UV regions. The higher the absorption over these three regions is, the higher the efficiency. The response of the solar absorber can be increased by integrating metasurfaces and graphene in the design. The metamaterial solar absorbers are effective and improve efficiency to a great extent because of their negative refraction.

Metamaterial solar absorbers are widely used to obtain a wideband result in spectrum regions [1]. Metasurface-based designs are also applicable in solar thermal conversion. The absorber shows broadband response with near-unity absorption with a tungsten-based

resonating surface [2]. The metamaterial absorber with a grating resonating structure shows an average of 90% absorption but this absorber does not cover the ultraviolet region [3]. The solar absorber design with square and circle metasurface absorbers is used for achieving broadband absorption. The absorber design can absorb most of the near-infrared region energy [4]. A broadband metamaterial absorber is designed to absorb the solar spectrum in the visible region [5]. Ultrabroadband response covering the solar spectrum is achieved by using a slotted square-shaped resonator over a dielectric substrate [6]. A graphene metamaterial sawtooth structure-based solar absorber is presented in [7]. A perfect absorber for absorbing visible energy of the solar spectrum is designed with broad response and polarization and angle insensitiveness [8,9]. The perfect unity absorber was designed using metamaterial for absorbing the soslar spectrum visible energy. The designed absorber can be applicable in thermal imaging applications [10]. Metamaterial absorbers are gaining interest amongst researchers and are currently widely researched. The absorber structure based on a single resonator is presented in [11]. Dual-band absorber and perfect absorber based on metamaterial are given in [12,13]. The absorber structure based on gallium arsenide substrate is designed for the perfect absorber using a metamaterial resonating structure [14]. Graphene is another material that can be placed in solar absorbers to improve its absorption.

Graphene is single-atom-thick graphite used in the solar absorber to improve its wideband response. Graphene and graphene oxides are most popular amongst researchers because of their high-conducting nature and good electrical and optical behavior. Graphene aerosols are also effective in increasing the heat which results in effective solar teams generation [15]. Graphene is also very effective in coating a solar absorber for anticorrosive effects [16]. The performance improvement in the greenhouse dryer is made with a solar absorber. It is possible to improve the performance of the dryer by painting the walls of the solar absorber with graphene coatings [17]. Graphene-based broadband absorbers are used to absorb most of the solar radiation [18–20]. Graphene-based metamaterial absorbers utilize the metamaterial resonator over a dielectric or metal substrate and sandwich a graphene layer between them which increases the efficiency and increases overall bandwidth [21–23]. Graphene-based absorbers are also used for perfect absorption in the terahertz spectrum [24].

The need for high absorption in solar absorbers creates room for broadband solar absorbers with high absorption in all the solar spectrum regions. We have presented a broadband absorber having absorption over all three regions. The absorber is created using a multilayer approach of stacking substrate and resonator. Three substrates and three metasurface resonators having the same size and structure are stacked over one another respectively. All the parameters are optimized for getting better solutions and results. The absorption responses of the three designs are analyzed and compared. The design responses are analyzed with other similar designs too. The design, its responses, and conclusions are given in different sections as follows.

2. Multilayer Design

There are several solar absorber designs based on a single-layer approach but the need to increase efficiency has created a way to add more layers to improve absorption. One way to make a multilayer design is stacking layers periodically which we did in this case as presented in Figure 1. We added three layers of substrate and a plus-shaped metamaterial periodically one over the other. The addition of these layers improves the absorption and overall efficiency of the solar absorber. The design schematic is presented in Figure 1 which shows the three different designs with the addition of these layers. The top view and front view show the single-layer approach which shows that the metamaterial resonator is placed over a SiO_2 substrate with a graphene spacer. The addition of layers increases the overall height of the design. The substrate thickness, metasurface thickness, and graphene spacer thickness are 2500 nm, 1000 nm, and 0.34 nm respectively. The length of the substrate layer is kept at 5000 nm which is also the same as its width. The second layer of substrate and

metasurface resonator is placed over the main resonator. Three layers are stacked one over another to create a multilayer design. The thickness of the resonator and substrate for all three layers is kept the same. All the parameters are optimized and optimized values are selected for making the high absorption in the solar absorber design. The graphene layer conductivity is obtained using [25] and given in Equations (1)–(4).

$$\varepsilon(\omega) = 1 + \frac{\sigma_s}{\varepsilon_0 \omega \Delta}. \tag{1}$$

$$\sigma_{intra} = \frac{-je^2 k_B T}{\pi \hbar^2 (\omega - j2\Gamma)} \left(\frac{\mu_c}{k_B T} + 2ln \left(e^{-\frac{\mu_c}{k_B T}} + 1 \right) \right). \tag{2}$$

$$\sigma_{inter} = \frac{-je^2}{4\pi \hbar} ln \left(\frac{2|\mu_c| - (\omega - j2\Gamma)\hbar}{2|\mu_c| + (\omega - j2\Gamma)\hbar} \right). \tag{3}$$

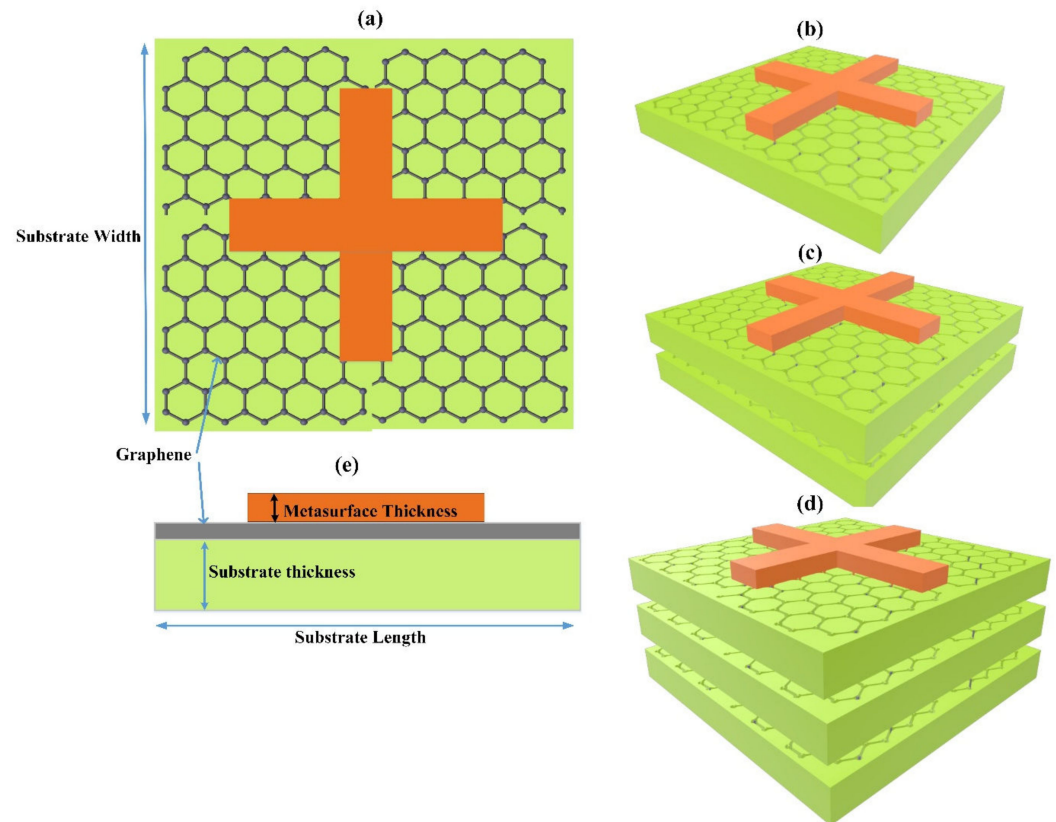$$\sigma_s = \sigma_{inter} + \sigma_{intra}. \tag{4}$$

Figure 1. Multilayer metamaterial design. (**a**) Plus-layer top view; (**b**) single layer; (**c**) two layers; (**d**) three layers; (**e**) single-layer front view. Three layers are added periodically one over the other with substrate and plus-shape metamaterial as a periodic component. Metasurface thickness is 1000 nm and substrate thickness is 2500 nm. Substrate length and width are kept at 5000 nm. The light is falling from the top of the structure.

The reflectance and absorption can be calculated from the following Equations (5)–(11) [25].

$$r(\omega, \theta_i) = \frac{\omega \cos \theta_i \prod_{00}(\omega, \theta_i)}{2i\hbar ck^2 + \omega \cos \theta_i \prod_{00}(\omega, \theta_i)}. \tag{5}$$

$$\sigma_{||}(\omega, k) = -i \frac{\omega}{4\pi \hbar k^2} \prod_{00}(\omega, k). \tag{6}$$

$$r(\omega, \theta_i) = \frac{2\pi \cos \theta_i \sigma_{||}(\omega, k)}{c + 2\pi \cos \theta_i \sigma_{||}(\omega, k)}. \tag{7}$$

$$\mathcal{R}(\omega, \theta_i) = |r(\omega, \theta_i)|^2. \tag{8}$$

$$\mathcal{R}(\omega, \theta_i) = \frac{4\pi^2 \cos^2\theta_i \left[\mathrm{Re}^2\sigma_{||}(\omega, k) + \mathrm{Im}^2\sigma_{||}(\omega, k) \right]}{\left[c + 2\pi\cos\theta_i\mathrm{Re}\sigma_{||}(\omega, k) \right]^2 + 4\pi^2\cos^2\theta_i\mathrm{Im}^2\sigma_{||}(\omega, k)}. \tag{9}$$

$$\mathcal{R}(\omega) = \mathcal{R}(\omega, 0) = \frac{4\pi^2 \left[\mathrm{Re}^2\sigma(\omega) + \mathrm{Im}^2\sigma(\omega) \right]}{\left[c + 2\pi\mathrm{Re}\sigma(\omega) \right]^2 + 4\pi^2\mathrm{Im}^2\sigma(\omega)}. \tag{10}$$

$$A(\omega) = 1 - \mathcal{R}(\omega) - T(\omega). \tag{11}$$

where *k* refers to the wave vector.

3. Multilayer Absorber Results

The multilayer design results are compared with single-layer and two-layer designs in this section to show the improvement in the overall efficiency of the design. Three different designs namely single-layer, two-layer, and three-layer designs are simulated using COMSOL Multiphysics. The design results are investigated using periodic boundary conditions with Delaunay tessellation and plane wave source. The light is falling from the top of the plus-shape metamaterial structure. The response comparison is given in Figure 2a. For the visible and ultraviolet ranges, the absorption is almost the same for all three absorbers but as we move toward the infrared range than the absorption is decreasing as the number of layers decreases. This clearly shows that the layer increase is affecting the solar absorption in the infrared range and the reason for this is the effective thickness of the structure is increasing by increasing the layers which are affecting the higher wavelength regions compared to the lower wavelength regions. The results of the three-layer design show the highest absorption of 93.8% in the visible spectrum, and 90% in the infrared spectrum with a wavelength of 700 to 2000 nm. The results of all three designs are compared in Table 1. Figure 2b shows the AM 1.5 response and a comparison of absorbed energy of multilayer solar absorber design is presented in green color. As presented in the results, the multilayer design is absorbing most of the solar spectral energy. The different colors in the AM 1.5 curve show the amount of energy absorbed. The green color shows the amount of energy absorbed from the solar radiation. There is only some energy missed which is shown with red color in the plot. The comparison of the absorption for three layer is carried out to show that the addition of the layer improves the absorption. This improvement in absorption increases the efficiency of the overall solar system. This improvement can be used where there are no size constraints on the design. One of the disadvantages of increasing the layers is its cost. The cost of the structure is increased by increasing the layers, thus where there are no constraints related to the size and cost, then this concept is lethal in improving the efficiency of the structure.

Table 1. Absorption comparison for visible and infrared region.

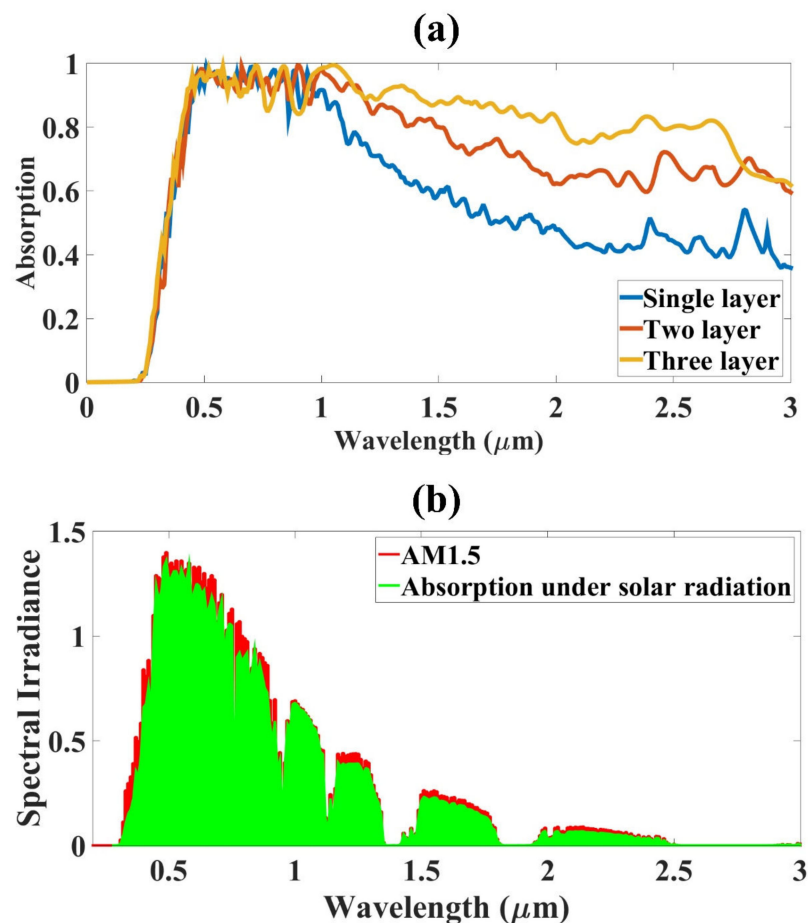| Design	Visible Band (400 to 700 nm) Absorption (%)	Infrared Band (701 to 2000 nm) Absorption (%)
Single-layer design	93	69
Two-layer design	92.6	82
Three-layer design	93.8	90

Figure 2. (**a**) Comparison of absorption results of single-layer design, two-layer design, and three-layer design is giving high absorption compared to the other two designs. The three-layer design (**b**) AM 1.5 results comparison with three-layer design results. The green color plot shows the absorption in the AM 1.5 response in W m^{-2} μm^{-1}. The red color shows the energy of AM 1.5 not absorbed through the absorber.

4. Structure Optimization of the Design

Optimization of the system can solve many problems which cannot be solved without it. The optimization of the system can be aimed at minimization of cost, energy consumption, etc. One of the important optimization methods is structural optimization. Structural optimization is important in improving the absorption of the solar absorber design. The structural optimization can be done with parametric optimization where parameters are optimized using parametric optimization algorithms. The parametric optimization algorithm is dependent on the behavior of the data which is sometimes having nonlinear constraints. The nonlinear optimization algorithm can be used in this case. The Nonlinear parametric optimization is one of the optimization algorithm which can be utilized to improve the nonlinear systems [26]. The nonlinear optimization algorithm is applied to microgrid to make the real-time operation which can be applicable in microgrid operations [27]. Optimization algorithms are also applicable in saving the energy in many industries by effectively scheduling the energy [28]. The dealing with constraints and applying the nonlinear optimization is presented in [29]. The detailed discussion about the nonlinear optimization is available in a book. A detailed investigation about constrained optimization algorithms and unconstrained optimization algorithm is in [30].

Nonlinear optimization is used when the function is not behaving linearly with respect to the variable. The nonlinear optimization has function $f(x)$, or constraint $c_i(x) = 1, 2, \ldots n$ or $d_j(x) = 0, 1, \ldots n$, are nonlinear functions of the vector of variables x.

Here in our research, we have applied variation to different parameter to maximize the absorption of the design. While doing this, we also have to consider the range of wavelength for which we are observing the behavior of absorption. The response which we are getting is nonlinear and thus this nonlinear optimization is applied to find out the best value of different parameters where the maximum absorption is achieved while considering the different wavelength range.

Optimization of the design is observed by varying structural parameters such as length, width, and height of substrate and metasurface thickness. The structure optimization is obtained by varying the different structural parameters to find out the optimized values of those structural parameters. In this section, we provide a detailed explanation of the optimization of each parameter. The structure optimization is presented in Figures 2–6. The variation is presented in a line plot as well as a color plot to show the high absorption region for different variations over 0 to 3000 nm. Metasurface thickness that is important structural parameter is observed between 500 to 1000 nm with a separation of 100 nm as presented in Figure 2. The increase in resonator thickness in increasing the absorption but for the initial wavelength range until 1000 nm the absorption is almost the same and it is changing after that point until 3000 nm. The increase in absorption is also the effect of an increase in the area of the resonator which makes the resonator absorb the light easily. The optimized quantity of the resonator thickness is 1000 nm. The initial wavelength range is showing minimum absorption until 0.3 μm. The absorption is increased after 0.3 μm and then it kept high absorption for the other spectrum range. The lineplot of absorption shows that, and the change in the resonator thickness changes the curve and optimized value of 1000 nm is achieved through nonlinear optimization algorithm and presented in the plot. The color plot also shows similar behavior and it is easy to understand the variation of energy though different colors. The blue color in the initial part shows the minimum solar energy absorption. The red part shows the maximum energy absorption. There are a few points in the wavelength where perfect absorption is achieved.

Substrate thickness is important in making the overall area of the structure a limited size. The substrate thickness is kept to a level that the overall area of the absorber should not be increased. The cost of the absorber will be increased if the substrate thickness is increased. The substrate thickness is observed at 1500 to 2500 nm with a separation of 250 nm as given in Figure 3. The rise in thickness increasing the absorption but for the initial wavelength range until 1000 nm, the absorption is almost the same and it is changed after that point until 3000 nm. The increase in absorption is also the effect of an increase in the area of the resonator which makes the resonator absorb the light easily. The substrate thickness increase is also important as it absorbs more energy. The increase in the substrate thickness to a certain extent is ok and not going to increase the cost of the absorber. The variation in the substrate thickness is limited to a minimum of 2500 nm because of this. Further increase to this thickness changes the inductance of the design and also increases the cost of the solar absorber structure.

The substrate length is observed at 5000 to 8000 nm with a separation of 1000 nm as presented in Figure 5. The increase in substrate length increases the absorption, but for the initial wavelength range until 2000 nm, the absorption is almost the same and it changes after that point until 3000 nm. This clearly shows that there is no effect in the UV and visible region, but the effect is visible in the higher infrared wavelength. The lesser the length, the greater the absorption in these higher infrared wavelengths. The substrate length is kept at 5000 nm with this optimization. As seen in the figure, the variation in the substrate length is not changing the absorption of the solar absorber design. The solar absorber was observed for different lengths and there is no variation in the results which show that the absorption is same. The increase in the thickness reduces the absorption for the higher wavelength region, and for the other lower wavelength region, it is almost the same.
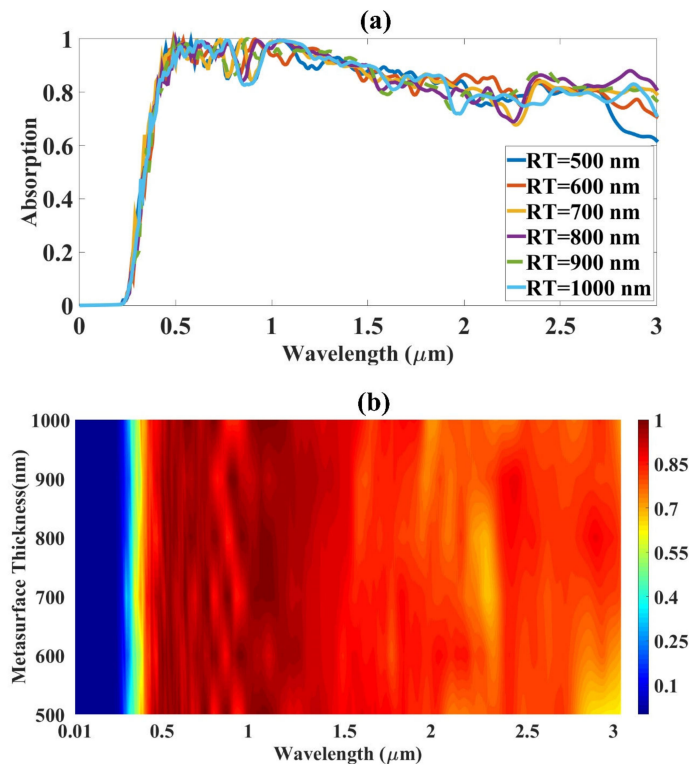
Figure 3. Absorption response for variation in RT (resonator thickness). Variation is carried out 500 to 1000 nm with a separation of 100 nm. The results are presented in the form of (**a**) line, (**b**) color plots for 0 to 3000 nm.
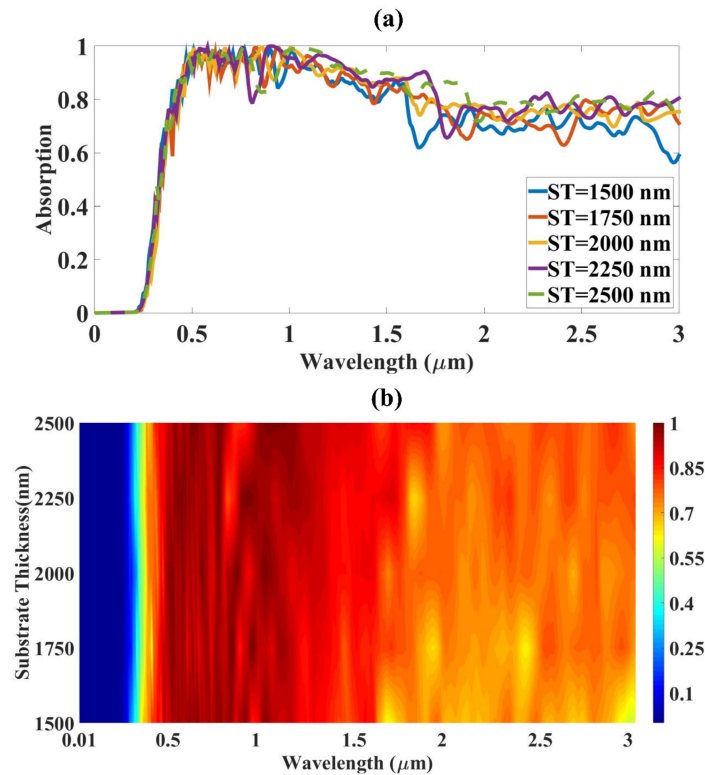

Figure 4. Absorption response for variation in ST (substrate thickness). The variation is carried out from 1500 to 2500 nm with a separation of 250 nm. The absorption spectrum is presented in the form of (**a**) line, (**b**) color plots for the wavelength range of 0 to 3000 nm.
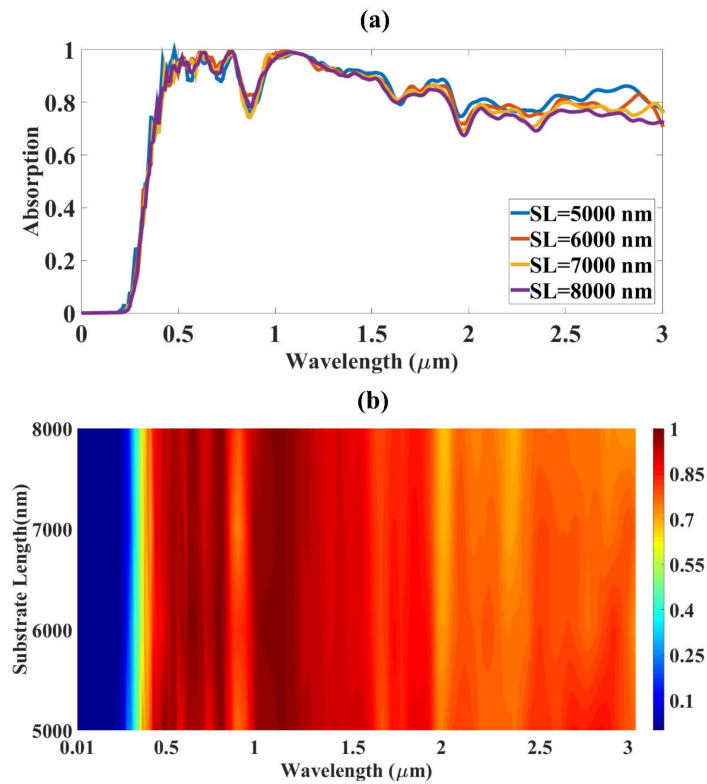
(a)

(b)

Figure 5. Absorption response for variation in SL (substrate length). The variation is carried out from 5000 to 8000 nm with a separation of 1000 nm. The absorption spectrum is presented in the form of (**a**) line, (**b**) color plots for 0 to 3000 nm.
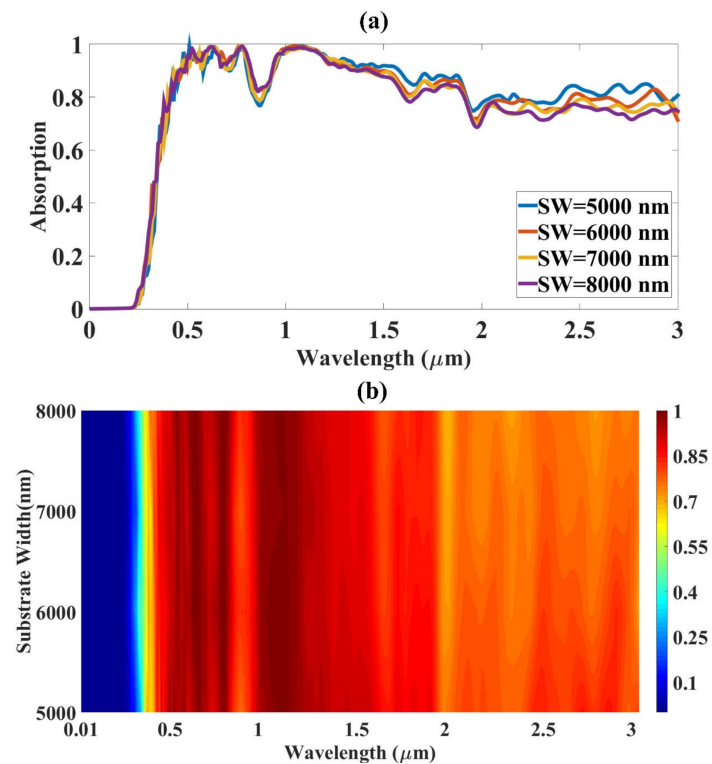
(a)

(b)

Figure 6. Absorption response for variation in SW (substrate width). The variation is carried out from 5000 nm to 8000 nm with a separation of 1000 nm. The absorption spectrum is presented in the form of (**a**) line, (**b**) color plots for 0 to 3000 nm.

The substrate width is observed at 5000 to 8000 nm with a separation of 1000 nm as presented in Figure 6. The increase in substrate width is increasing the absorption but for the initial wavelength range until 2000 nm, the absorption is almost the same and it changes after that point until 3000 nm. This clearly shows that there is no effect in the UV and visible region, but the effect is visible in the higher infrared wavelength. The lower the length, the more the absorption in these higher infrared wavelengths. The substrate width is kept at 5000 nm with this optimization. As seen in the figure, the variation in the substrate width does not change the absorption of the solar absorber design. The solar absorber is observed for different widths and there is no variation in the results, which shows that the absorption is same. The increase in the thickness is reducing the absorption for the higher wavelength region and for the other lower wavelength region it is almost the same. The color plot is clearly showing that the absorption is similar for almost all the variations. The absorption for the higher wavelength has some variation. The results of substate length and width are similar because our structure is square and has the same length and width. The same thing is also verified through these results.

Thus, after the structural optimization, the optimized values obtained were 1000 nm and 2500 nm for resonator thickness and substrate thickness, respectively. The length and width of the substrate were 5000 nm.

The comparison of the three responses with other published responses is shown in Table 2. The three-layer solar absorber showed better absorption in not only visible but also infrared regions. The electric field intensity response of the three-layer design is observed in Figure 7. The response clearly shows the high electric field intensity in visible and infrared wavelengths as is given in the absorption response shown in Figure 2. Both responses match well with each other, and it shows better similarity which verifies the results. The angular response is presented in Figure 8 which shows good absorption for different angles. The wide-angle results are given in the figure that shows the overall good response of the design. The E-field distribution is presented with absolute E-field (|E|) values. The E-field variation is verifying the absorption spectrum presented in Figure 2. The different wavelength E-field results matches with the absorption results. The red color in the field shows the high field while the blue color shows low electric field. The comparison with previously published results is presented in Table 2. The three-layer design results are compared with other designs. The absorption is compared for visible and infrared regions. The visible band is observed for 400 to 700 nm and infrared band is observed for 701 to 2000 nm. The highest absorption of 93.8% is available for visible region and 90% is available for infrared region.

Table 2. Comparison of published solar absorber designs with proposed plus-shape metasurface design.

Design	Visible Band (400 to 700 nm) Absorption (%)	Infrared Band (701 to 2000 nm) Absorption (%)
Single-layer design	93	69
Two-layer design	92.6	82
Three-layer design	93.8	90
[31]	90	-
[32]	86.5	-
[33]	93	-
[34]	90	-
[34]	90	-
[35]	80	-
[36]	71.1	-
[37]	70	-

Table 2. *Cont.*

Design	Visible Band (400 to 700 nm) Absorption (%)	Infrared Band (701 to 2000 nm) Absorption (%)
[38]	84	77
[39]	93.7	-
[40]	92	-
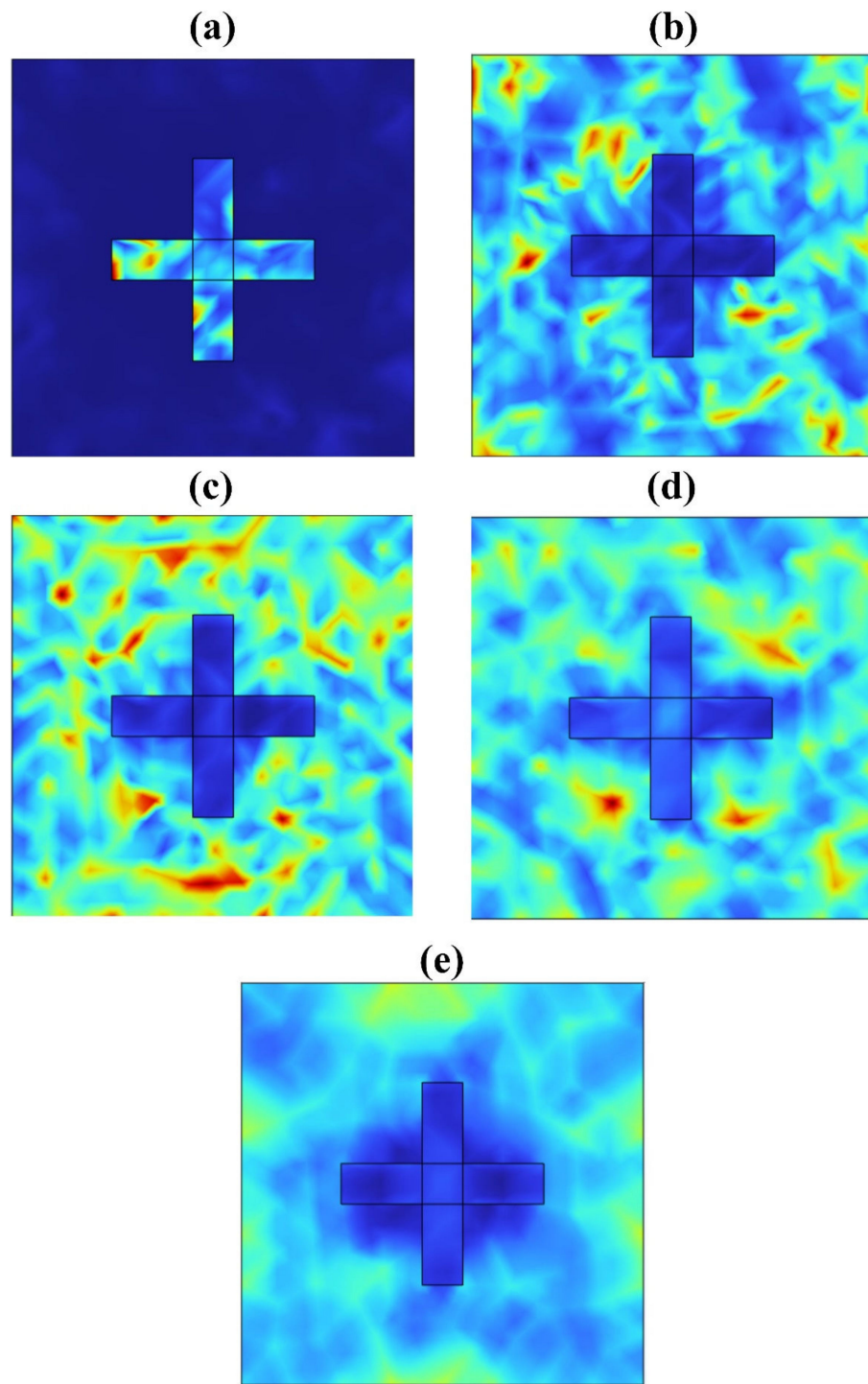
Figure 7. Electric field intensity (|E|) response for (**a**) 100 nm, (**b**) 400 nm, (**c**) 700 nm, (**d**) 1000 nm, and (**e**) 1500 nm.
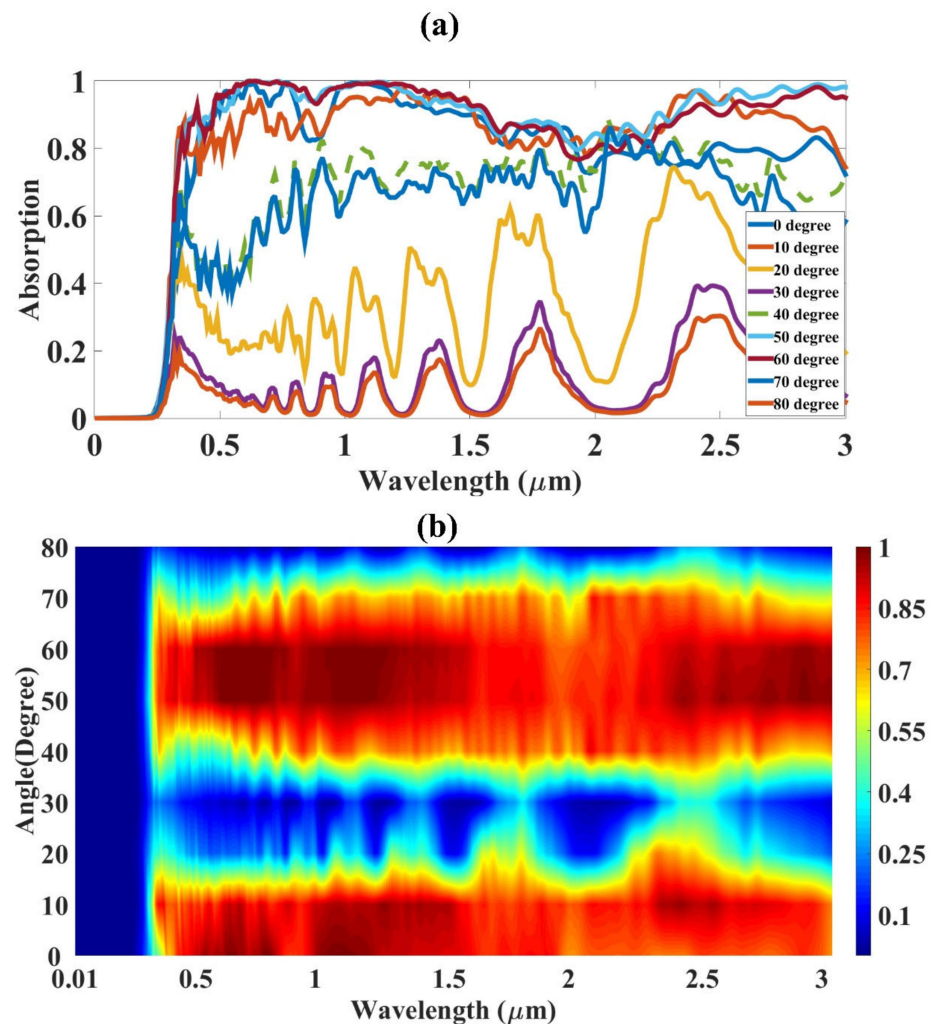
(a)

(b)

Figure 8. Angular response for 0 to 3000 nm range. (**a**) Line, (**b**) color plots for 0 to 80-degree angular response.

5. Conclusions

The numerical simulation and structural optimization of the solar absorber are presented to achieve high absorption. The multilayer approach in designing solar absorbers is analyzed in this manuscript. The multilayer design gives a better performance in visible and infrared regions compared to the single-layer design. The multilayer design shows 90% absorption in the infrared region of 701 nm to 2000 nm and 93.8% average absorption in the 400 nm to 700 nm visible region. Structural optimization gives the best absorption for the multilayer solar absorber design. The structural optimization shows optimized values of 1000 nm for resonator thickness, 2500 nm for substrate thickness, and 5000 nm for substrate length and width. The electric field response of the multilayer design also matches well with the achieved absorption results. The comparison with AM 1.5 spectral irradiance curve also shows that the absorber absorbs most of the solar radiation.

Author Contributions: Conceptualization, H.A. and S.K.P.; methodology, H.A. and N.B.A.; software, S.K.P. and A.A.; validation, H.A., S.K.P. and N.B.A.; formal analysis, A.A. and K.A.; investigation, S.K.P. and A.A.; resources, H.A., S.K.P. and A.A.; writing—original draft preparation, all authors.; writing—review and editing, S.K.P.; visualization, N.B.A.; supervision, N.B.A.; project administration; funding acquisition, H.A. and N.B.A. All authors have read and agreed to the published version of the manuscript.

Data Availability Statement: The data will be made available upon reasonable request to the corresponding author.

Conflicts of Interest: The authors declare no conflict of interest.

References

1. Hoque, A.; Islam, M.T.; Almutairi, A.F.; Faruque, M.R.I. Design of Split Hexagonal Patch Array Shaped Nano-metaabsorber with Ultra-wideband Absorption for Visible and UV Spectrum Application. *Nanoscale Res. Lett.* **2019**, *14*, 393. [CrossRef] [PubMed]
2. Chang, C.-C.; Kort-Kamp, W.J.M.; Nogan, J.; Luk, T.S.; Azad, A.K.; Taylor, A.J.; Dalvit, D.A.R.; Sykora, M.; Chen, H.-T. High-Temperature Refractory Metasurfaces for Solar Thermophotovoltaic Energy Harvesting. *Nano Lett.* **2018**, *18*, 7665–7673. [CrossRef]
3. Nguyen, D.M.; Lee, D.; Rho, J. Control of light absorbance using plasmonic grating based perfect absorber at visible and near-infrared wavelengths. *Sci. Rep.* **2017**, *7*, 2611. [CrossRef] [PubMed]
4. Patel, S.K.; Parmar, J.; Katrodiya, D.; Nguyen, T.K.; Holdengreber, E.; Dhasarathan, V. Broadband metamaterial-based near-infrared absorber using an array of uniformly placed gold resonators. *J. Opt. Soc. Am. B* **2020**, *37*, 2163–2170. [CrossRef]
5. Hoque, A.; Islam, M.T. Numerical Analysis of Single Negative Broadband Metamaterial Absorber Based on Tri Thin Layer Material in Visible Spectrum for Solar Cell Energy Harvesting. *Plasmonics* **2020**, *15*, 1061–1069. [CrossRef]
6. Feng, H.; Xu, Z.; Li, K.; Wang, M.; Xie, W.; Luo, Q.; Chen, B.; Kong, W.; Yun, M. Tunable polarization-independent and angle-insensitive broadband terahertz absorber with graphene metamaterials. *Opt. Express* **2021**, *29*, 7158–7167. [CrossRef]
7. Lin, K.-T.; Lin, H.; Yang, T.; Jia, B. Structured graphene metamaterial selective absorbers for high efficiency and omnidirectional solar thermal energy conversion. *Nat. Commun.* **2020**, *11*, 904–909. [CrossRef]
8. Sekhi, S.Z.; Shokooh-Saremi, M.; Mirsalehi, M.M. Ultra-broadband, wide-angle, and polarization-insensitive metamaterial perfect absorber for solar energy harvesting. *J. Nanophotonics* **2020**, *14*, 046014. [CrossRef]
9. Zhou, J.; Liu, X.; Zhang, H.; Liu, M.; Yi, Q.; Liu, Z.; Wang, J. Cross-Shaped Titanium Resonators Based Metasurface for Ultra-Broadband Solar Absorption. *IEEE Photon. J.* **2021**, *13*, 1–8. [CrossRef]
10. Cheng, Y.; Du, C. Broadband plasmonic absorber based on all silicon nanostructure resonators in visible region. *Opt. Mater.* **2019**, *98*, 109441. [CrossRef]
11. Cheng, Y.; Zhao, J. Simple design of a six-band terahertz perfect metasurface absorber based on a single resonator structure. *Phys. Scr.* **2022**, *97*, 95508. [CrossRef]
12. Li, Z.; Cheng, Y.; Luo, H.; Chen, F.; Li, X. Dual-Band Tunable Terahertz Perfect Absorber Based on All-Dielectric InSb Resonator Structure for Sensing Application. *J. Alloys Compd.* **2022**, *925*, 166617. [CrossRef]
13. Zhao, J.; Cheng, Y. Temperature-Tunable Terahertz Perfect Absorber Based on All-Dielectric Strontium Titanate (STO) Resonator Structure. *Adv. Theory Simul.* **2022**, *5*, 2200520. [CrossRef]
14. Cheng, Y.; Qian, Y.; Luo, H.; Chen, F.; Cheng, Z. Terahertz Narrowband Perfect Metasurface Absorber Based on Micro-Ring-Shaped GaAs Array for Enhanced Refractive Index Sensing. *Phys. E LowDimens. Syst. Nanostruct.* **2023**, *146*, 115527. [CrossRef]
15. Fu, Y.; Wang, G.; Ming, X.; Liu, X.; Hou, B.; Mei, T.; Li, J.; Wang, J.; Wang, X. Oxygen plasma treated graphene aerogel as a solar absorber for rapid and efficient solar steam generation. *Carbon* **2018**, *130*, 250–256. [CrossRef]
16. Šest, E.; Dražič, G.; Genorio, B.; Jerman, I. Graphene nanoplatelets as an anticorrosion additive for solar absorber coatings. *Sol. Energy Mater. Sol. Cells* **2018**, *176*, 19–29. [CrossRef]
17. Selimefendigil, F.; Şirin, C.; Öztop, H.F. Improving the performance of an active greenhouse dryer by integrating a solar absorber north wall coated with graphene nanoplatelet-embedded black paint. *Sol. Energy* **2022**, *231*, 140–148. [CrossRef]
18. Huang, H.; Xia, H.; Xie, W.; Guo, Z.; Li, H.; Xie, D. Design of broadband graphene-metamaterial absorbers for permittivity sensing at mid-infrared regions. *Sci. Rep.* **2018**, *8*, 4183. [CrossRef]
19. Safaei, M.R.; Goshayeshi, H.R.; Chaer, I. Solar Still Efficiency Enhancement by Using Graphene Oxide/Paraffin Nano-PCM. *Energies* **2019**, *12*, 2002. [CrossRef]
20. Cen, C.; Chen, Z.; Xu, D.; Jiang, L.; Chen, X.; Yi, Z.; Wu, P.; Li, G.; Yi, Y. High Quality Factor, High Sensitivity Metamaterial Graphene—Perfect Absorber Based on Critical Coupling Theory and Impedance Matching. *Nanomaterials* **2020**, *10*, 95. [CrossRef]
21. Ogawa, S.; Shimatani, M.; Fukushima, S.; Okuda, S.; Matsumoto, K. Graphene on metal-insulator-metal-based plasmonic metamaterials at infrared wavelengths. *Optics Express* **2018**, *26*, 5665–5674. [CrossRef] [PubMed]
22. Lakshmiprabha, K.E.; Govindaraju, C.; Mahendran, G. Broadband plus-Shaped Metasurface Absorber Based on Graphene for Visible and Ultraviolet Regions. *Opt. Quantum Electron.* **2022**, *54*, 774. [CrossRef]
23. Rezk, H.; Ali, Z.M.; Abdalla, O.; Younis, O.; Gomaa, M.R.; Hashim, M. Hybrid Moth-Flame Optimization Algorithm and Incremental Conductance for Tracking Maximum Power of Solar PV/Thermoelectric System under Different Conditions. *Mathematics* **2019**, *7*, 875. [CrossRef]
24. Zhu, J.; Wu, C.; Ren, Y. Broadband terahertz metamaterial absorber based on graphene resonators with perfect absorption. *Results Phys.* **2021**, *26*, 104466. [CrossRef]

25. Patel, S.K.; Surve, J.; Parmar, J.; Nguyen, T.K. Review on Graphene-Based Absorbers for Infrared to Ultraviolet Frequencies. *J. Adv. Eng. Comput.* **2021**, *5*, 214. [CrossRef]

26. Yang, X.-S. Nature-inspired optimization algorithms: Challenges and open problems. *J. Comput. Sci.* **2020**, *46*, 101104. [CrossRef]

27. Shuai, H.; Fang, J.; Ai, X.; Wen, J.; He, H. Optimal Real-Time Operation Strategy for Microgrid: An ADP-Based Stochastic Nonlinear Optimization Approach. *IEEE Trans. Sustain. Energy* **2018**, *10*, 931–942. [CrossRef]

28. Jiang, T.; Zhang, C.; Zhu, H.; Gu, J.; Deng, G. Energy-Efficient Scheduling for a Job Shop Using an Improved Whale Optimization Algorithm. *Mathematics* **2018**, *6*, 220. [CrossRef]

29. Yang, X.-S. How to Deal with Constraints. In *Nature-Inspired Optimization Algorithms*; Elsevier: Amsterdam, The Netherlands, 2021; pp. 207–220.

30. Aragón, F.J.; Goberna, M.A.; López, M.A.; Rodríguez, M.M.L. *Nonlinear Optimization (Springer Undergraduate Texts in Mathematics and Technology)*; Springer International Publishing: Cham, Switzerland, 2019.

31. Yu, P.; Chen, X.; Yi, Z.; Tang, Y.; Yang, H.; Zhou, Z.; Duan, T.; Cheng, S.; Zhang, J.; Yi, Y. A numerical research of wideband solar absorber based on refractory metal from visible to near infrared. *Opt. Mater.* **2019**, *97*, 109400. [CrossRef]

32. Patel, S.K.; Charola, S.; Parmar, J.; Ladumor, M.; Ngo, Q.M.; Dhasarathan, V. Broadband and Efficient Graphene Solar Absorber Using Periodical Array of C-Shaped Metasurface. *Opt. Quantum Electron.* **2020**, *52*, 250. [CrossRef]

33. Lin, H.; Sturmberg, B.C.P.; Lin, K.-T.; Yang, Y.; Zheng, X.; Chong, T.K.; de Sterke, C.M.; Jia, B. A 90-nm-thick graphene metamaterial for strong and extremely broadband absorption of unpolarized light. *Nat. Photonics* **2019**, *13*, 270–276. [CrossRef]

34. Azad, A.K.; Kort-Kamp, W.J.M.; Sykora, M.; Weisse-Bernstein, N.R.; Luk, T.S.; Taylor, A.J.; Dalvit, D.A.R.; Chen, H.-T. Metasurface Broadband Solar Absorber. *Sci. Rep.* **2016**, *6*, 20347. [CrossRef]

35. Liu, B.; Tang, C.; Chen, J.; Xie, N.; Tang, H.; Zhu, X.; Park, G.-S. Multiband and Broadband Absorption Enhancement of Monolayer Graphene at Optical Frequencies from Multiple Magnetic Dipole Resonances in Metamaterials. *Nanoscale Res. Lett.* **2018**, *13*, 153. [CrossRef]

36. Sang, T.; Gao, J.; Yin, X.; Qi, H.; Wang, L.; Jiao, H. Angle-Insensitive Broadband Absorption Enhancement of Graphene Using a Multi-Grooved Metasurface. *Nanoscale Res. Lett.* **2019**, *14*, 105. [CrossRef]

37. Rufangura, P.; Sabah, C. Graphene-Based Wideband Metamaterial Absorber for Solar Cells Application. *J. Nanophotonics* **2017**, *11*, 036008. [CrossRef]

38. Liu, Y.; Chen, Y.; Li, J.; Hung, T.-C.; Li, J. Study of energy absorption on solar cell using metamaterials. *Sol. Energy* **2012**, *86*, 1586–1599. [CrossRef]

39. Patel, S.K.; Charola, S.; Parmar, J.; Ladumor, M. Broadband metasurface solar absorber in the visible and near-infrared region. *Mater. Res. Express* **2019**, *6*, 086213. [CrossRef]

40. Katrodiya, D.; Jani, C.; Sorathiya, V.; Patel, S.K. Metasurface based broadband solar absorber. *Opt. Mater.* **2019**, *89*, 34–41. [CrossRef]